Inorganic Chemistry

Article

pubs.acs.org/IC

Synthesis and Properties of Multifunctional Tetragonal Eu:$GdPO_4$ Nanocubes for Optical and Magnetic Resonance Imaging Applications

Sonia Rodriguez-Liviano,[†] Ana I. Becerro,[†] David Alcántara,[‡] Valeria Grazú,[‡] Jesus M. de la Fuente,[‡] and Manuel Ocaña*,[†]

[†]Instituto de Ciencia de Materiales de Sevilla (CSIC-US), Americo Vespucio 49, Isla de La Cartuja, 41092 Sevilla, Spain

[‡]Instituto de Nanociencia de Aragon, Universidad de Zaragoza, Mariano Esquillor s/n, Zaragoza, 50018, Zaragoza, Spain

Supporting Information

ABSTRACT: A simple and fast (7 min) procedure for synthesis of gadolinium phosphate nanocubes (edge = 75 nm) based on the microwave-assisted heating at 120 °C of gadolinium acetylacetonate and phosphoric acid solutions in buthylene glycol is reported. These nanocubes were highly crystalline and crystallized into a tetragonal structure, which has not been ever reported for pure gadolinium phosphate. Determination of such crystal structure has been carried out here for the first time in the literature by means of powder X-ray diffraction. The developed synthesis procedure was also successful for preparation of multifunctional europium(III)-doped the gadolinium phosphate nanocubes, which were nontoxic for cells and exhibited strong red luminescence under UV illumination and high transverse relaxivity (r_2) values. These properties confer them potential applications as biolabels for in vitro optical imaging and as negative contrast agent for magnetic resonance imaging.

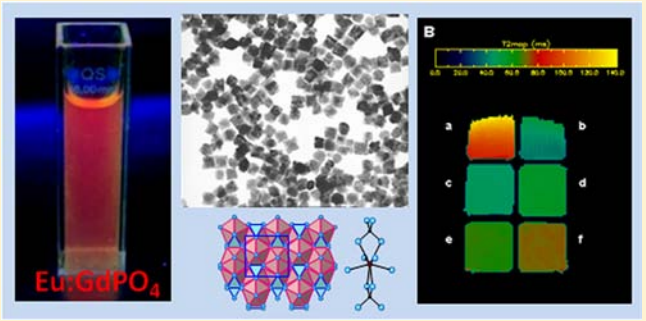

INTRODUCTION

During the past decade, much attention has been paid in the biomedical field to development of multifunctional nanostructures having several capabilities (imaging, targeting, drug delivery, etc.)[1] owing to the obvious advantages that they present over the systems with a single functionality. Among these multifunctional nanomaterials, those suitable for both optical and magnetic resonance (MRI) imaging are of special interest[1e,2] since they combine the high sensitivity of optical imaging for in vitro applications with excellent spatial resolution and depth for in vivo application associated to the MRI imaging.[2b,c,f,g] A large variety of architectures (core−shell nanoparticles,[1d,2f] nanocrystals of the different components attached[1f] or embedded in different matrices,[1b,3] superparamagnetic nanoparticles doped with luminescent ions[4] or dyes,[5] etc.), and compositions have been proposed. In such materials, the optical functionality is usually afforded by quantum dots,[2a] fluorescent dyes,[2a,5] or rare-earth-based compounds,[2b−i,3] the latter being preferred due to their lower toxicity and higher stability.[6] For the MRI functionality the most frequently used contrast agent is superparamagnetic iron oxide,[2a,f,3−6] although different kinds of nanoparticles containing Gd(III) ions are becoming very popular[2e,g,i,7] since these cations are the ideal paramagnetic relaxation agents due to their large magnetic moment and nanosecond time scale electronic relaxation time.[8] These Gd-containing materials may consist of a Gd(III) complex,[9] a diamagnetic matrix doped with Gd cations ions,[2b] or Gd compounds such as Gd_2O_3,[1e,2c,i,7] GdF_3,[8] and $NaGdF_4$[2c,e,g,h] to mention a few. Important advantages of the latter systems compared with the Gd(III) complexes are a dramatic increase in the local Gd ion concentration at the region of interest, easy functionalization, control of targeting and release through their particle size, and possibility of improved relaxivities.[2g]

To the best of our knowledge, most Gd-based systems evaluated as dual-imaging probes are based on lanthanide-doped (Er,Yb,Gd) fluorides ($NaLnF_4$, Ln = Gd or Na)[2b,d,e,h] or Gd_2O_3 doped with either organic dyes[7] or lanthanide (Tb, Er, Yb) ions.[1e,2c,i] However, other Gd compounds have been also suggested as good candidates for MRI applications such as $GdPO_4$,[10] which has been shown to present better performance than some commercial contrast agents such as Magnevist (gadolinium diethylenetriaminepentaacetic acid).[10a]

It should be noted that several procedures have been reported for synthesis of $GdPO_4$ nanoparticles, most of them leading to long (>500 nm) nanowires or nanorods,[11] which are not suitable for in vivo applications, which require sizes < 100 nm.[12] Only a few methods have been developed to produce smaller nanoparticles, which resulted in nanohexagons (15

Received: August 2, 2012
Published: December 26, 2012

   dx.doi.org/10.1021/ic3016996 | *Inorg. Chem.* 2013, 52, 647−654

nm),[13] nanorods (length ≈ 50 nm),[10c,14] or less uniform elongated nanoparticles (length = 100−200 nm)[10c,14] consisting of hexagonal or monoclinic $GdPO_4$.

Herein, we report a simple and fast (7 min) procedure for synthesis of multifunctional europium(III)-doped $GdPO_4$ nanocubes (~75 nm) and explore their suitability for optical and MRI bioimaging. For such a purpose, we optimized the luminescence properties of this material by adjusting the Eu doping level and evaluated the r_1 and r_2 relaxivities associated to the optimum nanoparticles and their citotoxicity. It is also outstanding that the obtained nanocubes crystallized into the tetragonal phase which, although it is a usual polymorph for small lanthanide (from Tb to Lu) phosphates,[15] has not been ever reported for pure $GdPO_4$. For this reason, we performed also a complete refinement of the crystal structure of this polymorph using powder X-ray diffraction and the Rietveld method.

EXPERIMENTAL SECTION

Reagents. Gadolinium(III) acetylacetonate hydrate ($Gd(C_5H_7O_2)_3{\cdot}xH_2O$, Aldrich, 99.9%), gadolium(III) nitrate hexahydrate ($Gd(NO_3)_3{\cdot}6H_2O$ (Aldrich, 99.9%), and europium acetylacetonate hydrate ($Eu(C_5H_7O_2)_3{\cdot}xH_2O$, Aldrich, 99.9%) were selected as lanthanide (Ln) precursors, whereas orthophosphoric acid (H_3PO_4, Aldrich, 85%) was the phosphate source. Butylene glycol (BG, Fluka, < 99.5%) and ethylene glycol (EG, Fluka, < 99.5%) were used as solvent.

Nanoparticles Synthesis. The standard procedure for synthesis of Eu:$GdPO_4$ nanocubes was as follows. Proper amounts of $Gd(acac)_3$ and $Eu(acac)_3$ were first dissolved in BG under magnetic stirring while heating at low temperature (~75 °C) to favor dissolution. After cooling to room temperature, concentrated phosphoric acid was added to such solutions so that its final concentration was 0.15 mol dm^{-3} (total volume = 10 cm^3). Lanthanide ions (Gd+Eu) concentration was 0.02 mol dm^{-3} in all experiments unless otherwise specified, whereas the Eu/Eu+Gd ratio was varied in order to investigate the effect of this parameter on the morphological and luminescent properties of the precipitated nanoparticles. After homogenization, a slight turbidity appeared that was found to be due to an amorphous gel-like preciopitate. These final dispersions, placed in tightly closed reactors, were heated at 120 °C in a microwave (MW) oven (Sineo MDS-8) using a heating rate of 14 °C min^{-1} and kept at this temperature for 1 h. The resulting dispersions were cooled down to room temperature, centrifuged to remove the supernatants, and washed twice with ethanol and once with double-distilled water. Finally, the precipitates were dispersed in Milli-Q water. For specific analyses, the powders were dried at room temperature.

For comparison, some experiments were performed using a convection oven for heating or ethylene glycol as solvent.

Characterization. Particle shape was examined by transmission (TEM, Philips 200CM) electron microscopy. Particle size distributions were obtained by counting several hundreds of particles from the TEM micrographs.

The quantitative composition of the samples was analyzed by inductively coupled plasma atomic emission spectroscopy (ICP-AES, Horiba Jobin Yvon, Ultima 2).

The crystalline structure of the prepared samples was assessed from X-ray diffraction patterns (XRD, Panalytical, X'Pert Prowith an X-Celerator detector) collected at intervals of 0.02° (2θ) and an accumulation time of 4000 s. Crystallite size was obtained from the (200) XRD reflection (2θ at ~25.7°) using the Scherrer formula. Crystal structure refinement was carried out using the Rietveld method with the TOPAS software (TOPAS version 4.2, Bruker AXS, 2009). Starting parameters were those described for $TbPO_4$.[16] Refined parameters were background coefficients, zero error, scale factor, surface roughness, unit cell parameters, atom positions, isotropic temperature factors of Gd and P, and Lorentzian and Gaussian components of the crystallite size and strains. A TCHZ (Thompson-Cox-Hasting) function was used to describe the peak shape.

Infrared spectra (FTIR) of the nanophosphors diluted in KBr pellets were recorded in a Jasco FT/IR-6200 Fourier transform spectrometer. Thermogravimetric analyses (TGA) were performed in air at a heating rate of 10 °C min^{-1} using a Q600 TA Instrument.

Excitation and emission spectra of the nanophosphors dispersed in water (0.5 mg cm^{-3}) were recorded in a Horiba Jobin-Yvon Fluorolog3 spectrofluorometer operating in the front face mode. Lifetime measurements were obtained under pulsed excitation at 266 nm using the fourth harmonics of a Nd:YAG laser (Spectra Physics model DCR 2/2A 3378) with a pulse width of 10 ns and a repetition rate of 10 Hz. Fluorescence was analyzed through an ARC monochromator model SpectraPro 500-i and then detected synchronously with an EMI-9558QB photomultiplier and recorded by a Tektronix TDS420 digital oscilloscope.

Photographs showing the luminescence of the nanophosphors in water dispersions were taken under illumination with ultraviolet radiation (λ = 254 nm), filtered from a Hg discharge lamp.

Magnetic Relaxivity Measurements and MRI Phantom Analysis. ^1H NMR relaxation times T_1 and T_2 were measured at 9.4 T in a Bruker Biospec MRI unit and at 0.47 T in a Relaxiometer (Bruker Minispec spectrometer) at different concentrations of nanoparticles (0.1, 0.05, 0.025, 0.0125, and 0.00625 mg cm^{-3}) in water at 298K. T_1 and T_2 values were determined by the inversion−recovery method and the Carr−Purcell−Maiboom−Gill sequence, respectively. Images were postprocessed using dedicated IDL 6.2 (Exelis VIS Inc., Boulder, CA) software with homemade written scripts. Relaxivities $r_1(r_2)$ were obtained from the slopes of the curves $1/T_1(T_2)$ vs the concentration of Gd(III) expressed in millimolar.

Viability Testing. Cell viability and proliferation were analyzed by the MTT colorimetric assay.[17] For the cytotoxicity assay 5000 cells were seeded in each well of 96-well plates and grown for 24 h. After 24 h, the medium was replaced with fresh medium containing the nanoparticles in varying concentrations. After cultivation again for 24 h, 20 μL of MTT dye solution (5 mg/mL in PBS) was added to each well. After 3 h of incubation at 37 °C and 5% CO_2 the medium was removed, the cells were washed with fresh medium, and formazan crystals were dissolved in 100 μL of DMSO. The absorbance of each well was read on a microplate reader (Biotek ELX800) at 570 nm. The spectrophotometer was calibrated to zero absorbance using culture medium without cells. The relative cell viability (%) related to control wells containing cell culture medium without nanoparticles was calculated by $[A]_{test}/[A]_{control} \times 100$. Each measurement was repeated at least five times to obtain the mean values and standard deviation.

RESULTS AND DISCUSSION

Synthesis of $GdPO_4$ Nanoparticles. It is well known that uniform particles can be formed in solution by homogeneous precipitation, which can be achieved, for example, through slow and controlled release of the precipitating anions or cations in the reaction medium.[18] In this work, we selected the latter strategy using $Gd(acac)_3$ as Gd^{3+} reservoir, since these compounds can be dissolved in polyol media and further decomposed on heating such solutions, thus liberating the Ln^{3+} cations required for precipitation of $LnPO_4$ in the presence of phosphate anions.[19] It has been also documented that another requirement for precipitation of uniform particles is the separation of the nucleation and growth processes, which only occurs under a precise set of experimental conditions (reagents concentration, temperature, and aging time).[18] To establish such conditions for synthesis of our nanophosphors, we first addressed the undoped $GdPO_4$ system for simplicity.

It was found that the aging in a MW oven at 120 °C for 60 min of 0.02 mol dm^{-3} $Gd(acac)_3$ solutions in BG containing 0.15 mol dm^{-3} of H_3PO_4 conducted to homogeneous nanoparticles with cubic morphology and a mean edge dimension of 75 ± 10 nm (Figure 1), whose XRD pattern (Figure 2) has never been reported for any $GdPO_4$ phase.

dx.doi.org/10.1021/ic3016996 | Inorg. Chem. 2013, 52, 647−654

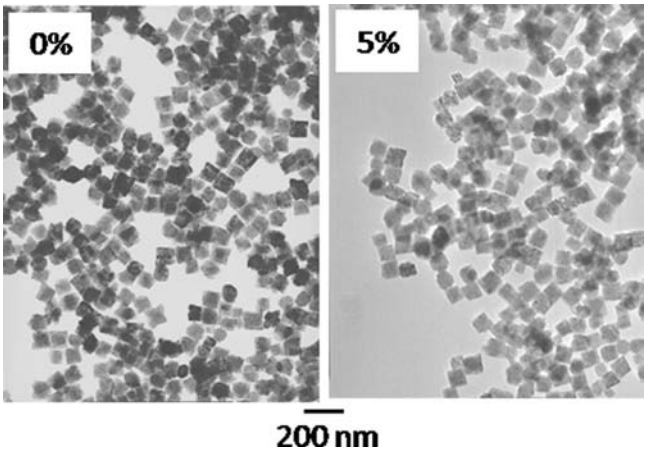

Figure 1. TEM images of the Eu:$GdPO_4$ nanoparticles prepared by heating at 120 °C for 1 h in a microwave oven and BG solutions containing H_3PO_4 (0.15 mol dm^{-3}) and $Eu(acac)_3$ and $Gd(acac)_3$ (Gd + Eu = 0.02 mol dm^{-3}) with different Eu content: 0% ($GdPO_4$) and 5% ($Eu_{0.05}Gd_{0.95}PO_4$).

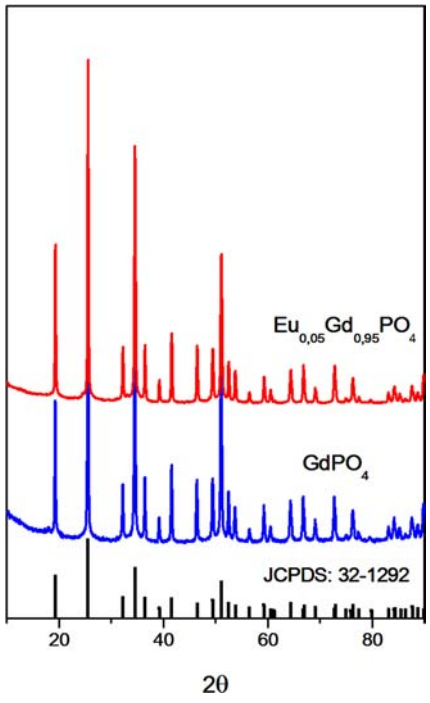

Figure 2. X-ray diffraction patterns recorded for samples shown in Figure 1. JCPDS file for tetragonal $TbPO_4$ is also included.

However, it was very similar to that of tetragonal $TbPO_4$ [PDF 00-032-1292, ICDD, 2011] appearing slightly shifted to lower 2θ values (higher interplanar spacing), suggesting a similar tetragonal symmetry for our $GdPO_4$ nanocubes. A detailed refinement of this tetragonal $GdPO_4$ phase will be given in the next section. The crystal size obtained from the (200) XRD reflection (assuming such structure) was almost identical (74 nm) to the edge of the nanocubes measured from the TEM micrographs (Table 1), suggesting that they were single crystals and that the crystallographic axes are parallel to the cube edges.

A summary of the effects of several experimental parameters on the morphological and structural characteristics of the precipitated particles is shown in Table 2. As observed, in this synthesis protocol the MW-assisted heating was essential since when keeping the same reagents concentrations and aging conditions but using a conventional oven (CH) for heating, long nanowires (Figure S1a, Supporting Information) with hexagonal structure (Figure S1b, Supporting Information) were obtained, although a very small amount of nanocubes was also present (Figure S1a, Supporting Information). To explain this different behavior, it must be taken into account that the heat transmission in the CH system is from the reactor wall to the inner wall creating a temperature gradient, whereas under MW irradiation, the OH groups of the polyol solvent absorb vast amounts of microwave energy, increasing rapidly the temperature of the system.[20] This results in a high reaction rate, as confirmed in a separate experiment which showed that nanocubes similar to those shown in Figure 1 were already formed after 7 min of MW-assisted aging. At such a fast kinetics, a single nucleation event would be favored, giving rise to formation of uniform particles, whereas a slower heating rate, such as that involved in a conventional heating, would give a chance for heterogeneous nucleation.

The nature of the polyol solvent was another key factor for formation of nanocubes. Thus, when BG was replaced by EG, a more heterogeneous sample composed by bigger spheroidal particles with heterogeneous size (Figure S2a, Supporting Information) was obtained, which consisted of a mixture of crystalline phases (tetragonal + monoclinic (Figure S2b, Supporting Information)).

These morphological differences are not surprising since the viscosity of BG is noticeably higher (71.5 MPs at 20 °C) than that of EG (18 MPs at 20 °C), which must affect the diffusion process required for nucleation and particle growth. It has been also reported that owing to the well-known complexing ability of polyols,[21] they may also act as complexing or capping agents. However, in our case, the presence of polyol species on the surface of the $GdPO_4$ nanocubes was not detected in the FTIR spectrum of the precipitated particles (Figure 3), which only showed several bands at <1250 cm^{-1} characteristic of the $GdPO_4$ lattice[14] along with two additional absorptions at 1630 and ~3400 cm^{-1}, which must be attributed to OH vibrations (bending and stretching, respectively) of adsorbed water. It should be noted that although the OH groups of BG molecules would also contribute to the OH stretching band as previously observed for Tb-doped $GdPO_4$ nanoparticles synthesized in EG,[14] the absence of peaks due to the CH_2 group of the polyol molecules (stretching vibrations at 2856 and 2927 cm^{-1} and bending vibration at 1460 cm^{-1}) discards the presence of BG molecules on the nanoparticles surface. Therefore, formation of stable complexes between the Gd cations and solvent molecules seems unlikely.

Table 1. Nominal and Experimental (ICP) Composition, Particle Size (Cube Edge), Crystal Size, Unit Cell Parameters, and Unit Cell Volume Measured for the $Eu_{0,05}Gd_{0,95}PO_4$ Nanocubes and for an Undoped $GdPO_4$ Sample

sample	Eu/Eu+Gd nominal (%)	Eu/Eu+Gd ICP (%)	cube edge (nm)	crystal size (nm)	$a = b$ (Å)	c (Å)	V (Å^3)
$GdPO_4$	0		75 ± 10	74	6.9648(4)	6.1050(5)	296.144
$Eu_{0.05}Gd_{0.95}PO_4$	5	4.98	71 ± 8		6.9698(2)	6.1094(2)	296.783

dx.doi.org/10.1021/ic3016996 | Inorg. Chem. 2013, 52, 647−654

Table 2. Effects of Different Experimental Parameters on the Morphological and Structural Characteristics of the Precipitated Particles[a]

[Gd] mol dm^{-3}	solvent	heating mode	morphology	particle size, nm	crystal phase
0.02	BG	microwave	cubes	75 ± 10	tetragonal
0.005	BG	microwave	cubes	79 ± 12	tetragonal
0.001	BG	microwave	cubes	120 ± 15	tetragonal
0.02	BG	microwave	gel-like		
0.02	BG	conventional	nanowires + cubes		hexagonal
0.02	EG	microwave	spheroidal	heterogeneous	tetragonal + monoclinic

[a]Constant conditions: H_3PO_4 concentration = 0.15 mol dm^{-3}, aging temperature = 120°C, aging time = 1 h.

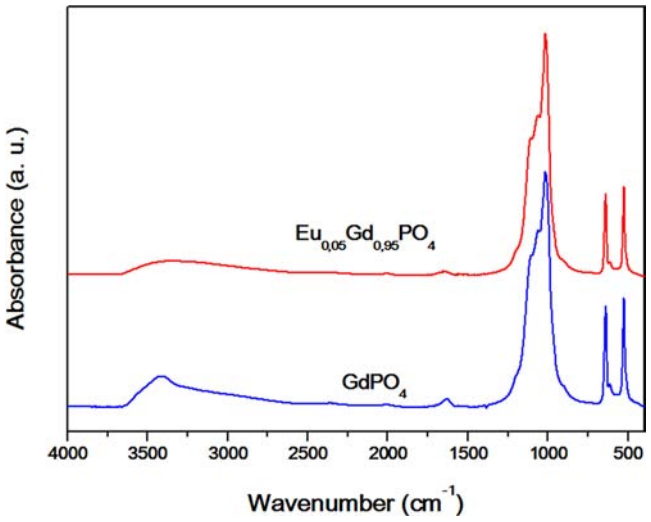

Figure 3. FTIR spectra recorded for samples shown in Figure 1.

It was also found that when the H_3PO_4 concentration was lowered from 0.15 to 0.05 mol dm^{-3}, keeping constant the other experimental parameters, only a slight turbidity associated to a gel-like precipitate was detected after aging, indicating a decrease of the precipitation rate, probably as a consequence of the decrease in the amount of phosphate anions available for precipitation. Therefore, at low H_3PO_4 concentration, the fast kinetics required for formation of GddPO$_4$ nanocubes cannot be reached. Finally, the decrease of Gd^{3+} concentration from 0.02 to 0.001 mol dm^{-3} gave rise to a progressive increase of particle size accompanied by certain shape heterogeneity (Figure S3, Supporting Information), whereas the Gd(acac)$_3$ precursor could not be completely dissolved at ≥0.05 mol dm^{-3}.

In summary, preparation of GdPO$_4$ nanocubes through the procedure reported here requires a very restrictive set of experimental conditions involving 0.02 mol dm^{-3} Gd(acac)$_3$ and 0.15 mol dm^{-3} H_3PO_4 solutions in BG and a MW-assisted heating at 120 °C.

Crystal Structure of Tetragonal GdPO$_4$. The rare-earth (RE; here considered as lanthanides + Y) phosphates, REPO$_4$, exist in nature as the phases monazite (monoclinic) and xenotime (tetragonal); less naturally abundant or synthetic phases are rhabdophane (hexagonal), weinschenkite (monoclinic), and orthorhombic.[22] Monazite incorporates the larger, light rare-earth elements (LREs, here La–Gd), whereas xenotime tends to incorporate the smaller, heavy rare-earth elements (HREs, here Tb–Lu + Y). Thus, Tb is the largest RE that the xenotime structure accommodates. To incorporate larger REs, a transition occurs from xenotime to monazite consisting of creation of a larger REO$_9$ polyhedron, the most common coordination for light REs, to be compared to the REO$_8$ polyhedra in the xenotime structure. In fact, the works of Milligan et al.[16,23] and later Ni et al.,[15] in their thorough report of high precision structure refinement of natural and synthetic monazite and xenotime phases, described the structural parameters of LnPO$_4$ monazite compounds with Ln = La–Gd and xenotime compounds with Ln = Tb–Lu. It should be noted that several authors have reported the stabilization of the tetragonal structure of GdPO$_4$ by substitution of part of the Gd atoms for smaller REs. Thus, Mullica et al.[24] reported the tetragonal structure of $Gd_{0.5}Yb_{0.5}PO_4$, while Mullica et al.[25] did so for $Gd_{0.75}Yb_{0.25}PO_4$, $Gd_{0.5}Er_{0.5}PO_4$, and $Gd_{0.5}Y_{0.5}PO_4$. Finally, Mullica et al.[26] described the tetragonal structure of $Gd_{0.5}Tb_{0.5}PO_4$ and $Gd_{0.75}Tb_{0.25}PO_4$. However, pure GdPO$_4$ with xenotime structure has never been reported to our knowledge.

We have shown that using the experimental approach described above, undoped GdPO$_4$ with the xenotime structure can be obtained. Using this sample, we refined the tetragonal GdPO$_4$ crystal structure for the first time in the literature from powder X-ray diffraction data by means of the Rietveld method with the TOPAS software (TOPAS version 4.2, Bruker AXS, 2009). As starting parameters we selected those reported for TbPO$_4$ by Milligan et al.[16] Figure 4a shows the experimental, fitted, and difference curves. All reflections could be fitted on the basis of a tetragonal cell with space group $I4_1/amd$. Space group $I4_1/amd$ has two origins: $-4md$ and $2/m$ (at the center). The latter origin (choice 2), which has two 4-fold positional sets, was chosen. Unit cell parameters obtained were a = 6.96632(11) Å and c = 6.11076(11) Å. Atomic parameters, interatomic distances, and agreement factors can be found in Table 3. Gd atoms are eight coordinate to the oxygen atoms with two unique Gd–O bond distances (2.3431(40) and 2.3974(37) Å). P atoms are tetrahedrally coordinated to the oxygen atoms with a unique P–O bond distance of 1.5543(38) Å and two different OPO angles (101.59(29)° and 113.55(15)°), forming, therefore, an irregular tetrahedron. The fundamental atomic arrangement of xenotime was first given by Vegard[27] for YPO$_4$, who described the structure as [001] chains formed of alternating Y polyhedra and phosphate tetrahedra. Figure 4b is a view of the structure along the a axis showing the polyhedron–tetrahedron chains. P tetrahedra are isolated with respect to other P tetrahedra, and they share two of their edges with the Gd polyhedra. On the other hand, each Gd polyhedron shares two edges with one another and two with the P tetrahedra. Finally, Figure 4c shows the unit cell volume described by Ni et al.[15] for the REPO$_4$(RE = Tb–Lu) xenotime phases versus the RE^{3+}(VIII) ionic radius as well as the two different RE–O distances and the unique RE–P distance. Data obtained in this work for GdPO$_4$ have been

dx.doi.org/10.1021/ic3016996 | Inorg. Chem. 2013, 52, 647–654

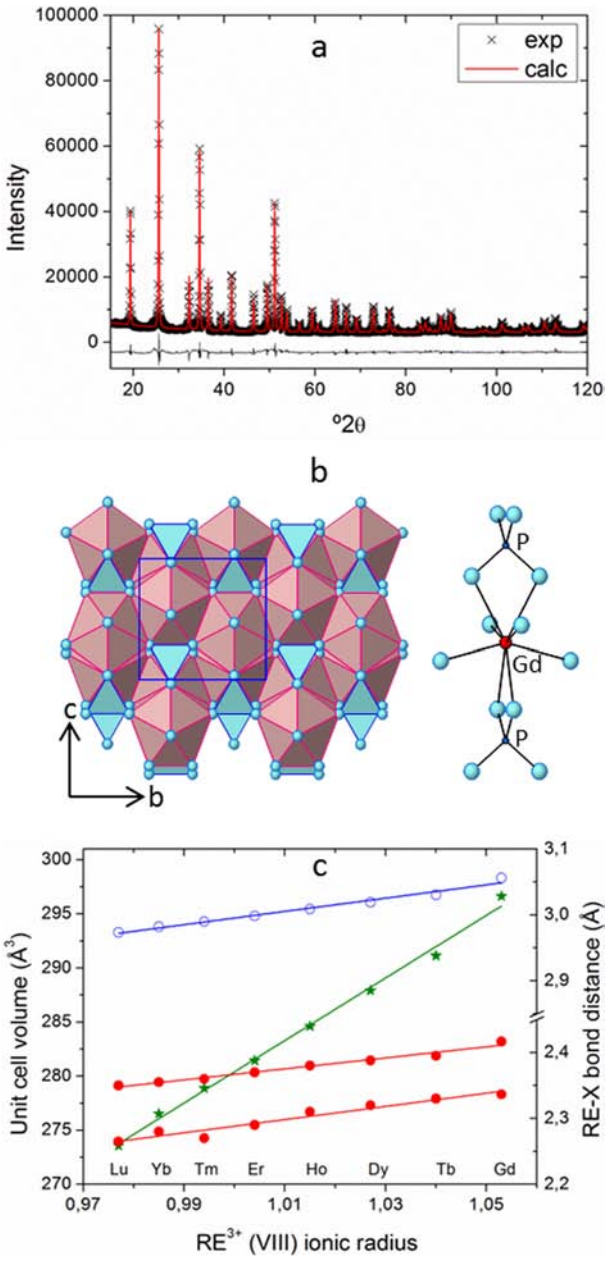

Figure 4. (a) Experimental (crosses) and fitted (solid line) XRD pattern of tetragonal $GdPO_4$. Difference curve is also shown. (b) View of the xenotime $GdPO_4$ structure along the [100] direction. Ball and stick picture shows the coordination of Gd and P to oxygen. (c) Unit cell volume (stars), RE–O (solid circles), and RE–P (open circles) bond distances in $REPO_4$ (RE = Lu–Tb) taken from Ni et al. (1995), and $GdPO_4$ data from this work.

Table 3. Refined Atomic Coordinates for $GdPO_4$ from X-ray Powder Diffraction Data Collected at RT[a]

site	*x*	*y*	*z*	Occ	B_{eq}
Gd	0.0000	0.7500	0.1250	1	0.75(4)
P	0.0000	0.2500	0.3750	1	0.11(8)
O	0.0000	0.4245(6)	0.2166(6)	1	0.00

[a]Space group $I4_1/amd$:2; a = 6.9670(1) Å and c = 6.1112(1) Å. R_{wp} = 5.31, GOF = 3.64.

added to the graph, and good agreement between our data and those of Ni et al. (1995) can be observed.

Synthesis and Properties of Eu-Doped $GdPO_4$ Nanophosphors. In order to optimize the luminescent properties of the Eu:$GdPO_4$ nanophosphors, several samples with different Eu content (Eu/Eu+Gd mol ratio = 2%, 5%, 8%, and 10%) were prepared starting from $Ln(acac)_3$ (Ln = Gd + Eu) solutions with the desired Eu/Gd ratio and keeping constant the other experimental conditions involved in the synthesis of the nanocubes shown in Figure 1. It was found that nanoparticles with similar size and shape as the undoped system were obtained if the Eu content was kept at ≤8%, as illustrated in Figure 1 and Table 1 for sample $Eu_{0.05}Gd_{0.95}PO_4$ whereas for higher values (≥10%) strong agglomeration was detected (Figure S4, Supporting Information). These agglomerated systems were discarded for further studies.

The presence of Eu in the doped particles was confirmed by chemical analyses, which showed that the experimental Eu/Eu+Gd ratio was very similar to the nominal values (Table 1). As illustrated for the $Eu_{0.05}Gd_{0.95}PO_4$ sample, doped nanocubes also crystallized into the tetragonal phase (Figure 2). Incorporation of the Eu cations into the $GdPO_4$ lattice was confirmed by the unit cell expansion detected for this sample when compared with the undoped nanoparticles (Table 1), in agreement with the differences in the ionic radius between Eu^{3+} (1.066 Å) and Gd^{3+} (1.053 Å) in VIII coordination.[28] The FTIR spectrum of the doped sample was also very similar to that of the undoped system (Figure 3), indicating that also in this case the only impurity contained in the nanoparticles was a certain amount of water and probably OH groups. TGA analysis revealed a weight loss of 3% in the 25–800 °C range (Figure S5, Supporting Information) corresponding to release of such impurities.

The excitation spectrum recorded for sample $Eu_{0.02}Gd_{0.98}PO_4$ (2% Eu content) by monitoring the Eu^{3+} emission at 618 nm (Figure 5, up) displayed a strong band at 273 nm along with much weaker features in the 300–400 nm range, among which the most intense appeared at 393 nm. The latter are due to direct excitation of the Eu^{3+} ground state to higher levels of the 4f manifold, whereas the former can be ascribed to the electronic transition from the ground state level of Gd^{3+} ($^8S_{7/2}$) to the $^6I_{11/2}$ excited levels,[29] which indicates that an energy transfer from Gd^{3+} multiplets to Eu^{3+} electronic levels takes place in this sample. It should be noted that the relative intensity of this energy transfer band with respect to those corresponding to direct excitation of the Eu cations is much higher than that previously observed for Eu:$GdPO_4$ particles with hexagonal[29] or monoclinic[30] structure, suggesting that such energy transfer is more efficient in tetragonal $GdPO_4$ and therefore that the Eu luminescence in the tetragonal polymorph should be more intense.

As observed in Figure 5 (bottom), excitation of the $Eu_{0.02}Gd_{0.98}PO_4$ sample at either 273 or 394 nm resulted in a similar emission spectrum, which presented several bands due to the $^5D_0$–^7F_J (J = 1, 2, 3, and 4) electronic transitions characteristic of the Eu^{3+}cations,[29,30] the most intense appearing in the 580–620 nm region, which are responsible for the strong orange-red luminescence (inset in Figure 5, bottom). In Figure 5 (bottom), it can be also observed that the intensity of the Eu^{3+} emissions was considerably higher when exciting through the Gd–Eu energy transfer band (λ_{ex} = 273 nm) than by direct excitation of the Eu^{3+} electronic levels (λ_{ex} = 394 nm), which is as expected from the excitation spectrum recorded for this sample.

dx.doi.org/10.1021/ic3016996 | Inorg. Chem. 2013, 52, 647–654

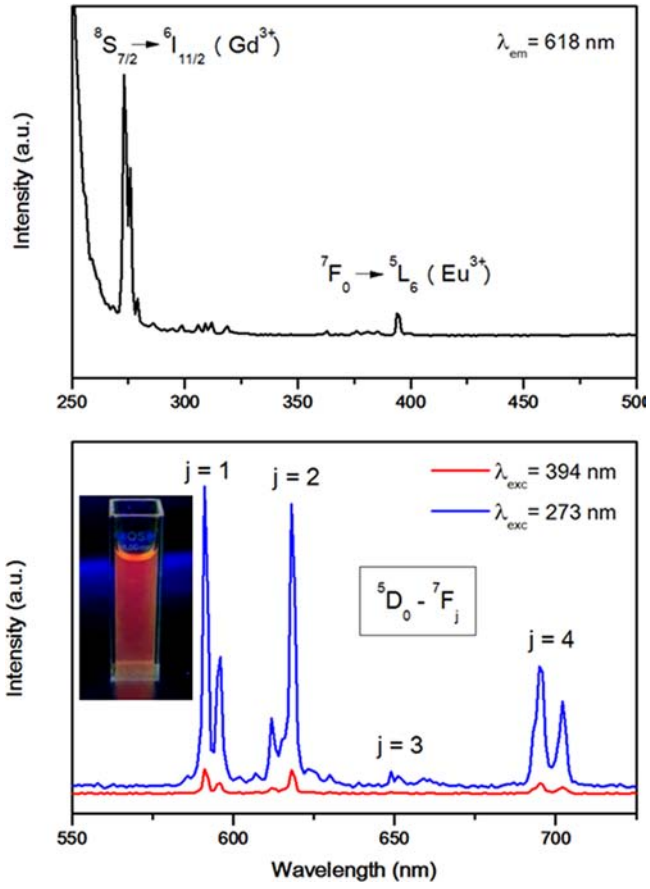

Figure 5. Excitation spectrum (λ_{em}= 618 nm) of the $Eu_{0.05}Gd_{0.95}PO_4$ sample (top), and emission spectra recorded for the same sample using different excitation wavelengths (bottom). (Inset) Photograph of a water suspension of the $Eu_{0.05}Gd_{0.95}PO_4$ nanophosphor taken under UV illumination.

Therefore, the effects of Eu content on the luminescence of the Eu:$GdPO_4$ nanocubes was studied for λ_{ex} = 273 nm. As expected, the emission spectra obtained for samples with Eu content ranging from 2% to 8% (Figure 6) displayed similar bands whose intensity slightly increased as increasing Eu

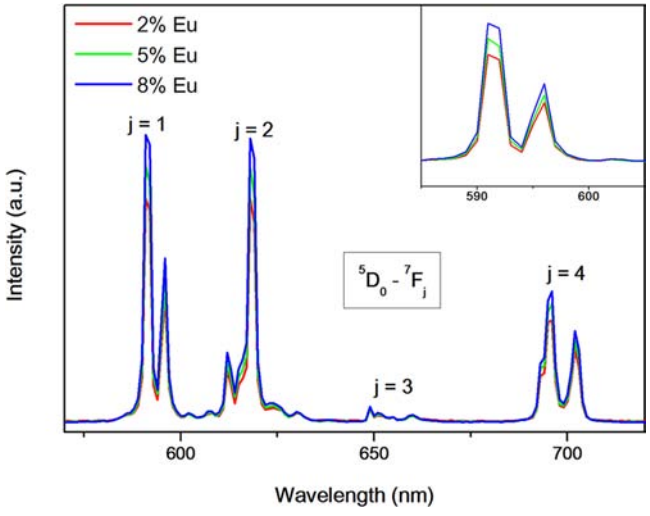

Figure 6. Emission spectra (λ_{em}= 273 nm) of the Eu:$GdPO_4$ samples with different Eu content.

content. In order to investigate a possible concentration quenching effect in these samples, luminescence lifetime measurements were carried out. The decay curves shown in Figure 7 were recorded at an emission wavelength of 618 nm

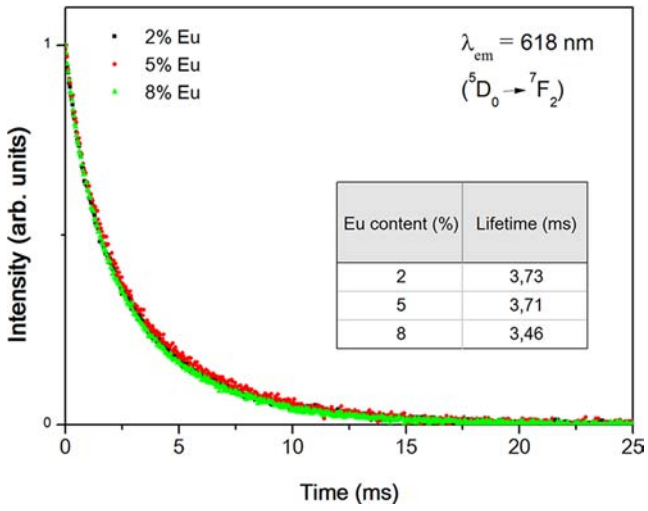

Figure 7. Decay curves obtained for the $^5D_0 \rightarrow {}^7F_2$ transition in the Eu:$GdPO_4$ samples having different Eu content after excitation at 266 nm and lifetimes obtained from these curves (inset).

($^5D_0 \rightarrow {}^7F_2$ transition), and the average lifetime values included in the inset of this figure were obtained from eq 1

$$\langle \tau \rangle = \frac{\int_0^\infty tI(t)\mathrm{d}t}{\int_0^\infty I(t)\mathrm{d}t} \quad (1)$$

As observed, τ remained almost constant (3.7 ms) when increasing the Eu content from 2% to 5%, whereas a decrease of this magnitude (3.46 ms) was detected when the Eu content was further increased to a 8%, indicating the presence of concentration quenching in the latter sample. Consequently, the most efficient Eu:$GdPO_4$ nanophosphors are those with an Eu content of 2−5%. Accordingly, $Eu_{0.02}Gd_{0.98}PO_4$ was used for evaluation of the magnetic relaxivities (r_1 and r_2) of this system in order to explore its potential applicability as MRI contrast agent.

Measurement of the longitudinal (T1) and transversal (T2) proton relaxation times as a function of the gadolinium ion concentration at 1.5 T gave for this sample r_1 and r_2 values of 0.19 and 17.33 S^{-1} mM^{-1}, respectively (Figure 8). It should be noted that these values are similar to those reported (measured at 14.1 T) for DNA surface-modified undoped hexagonal $GdPO_4$ nanorods having a length of 50 nm.[10b] The r_1 value is however much lower than that previously reported for smaller nanorods (~23 nm) of the same material coated with dextran polymers (13.9 S^{-1} mM^{-1}, measured at 7.05 T),[10a] which to the best of our knowledge is the highest value so far reported. This difference might be ascribed to a particle size effect. Thus, it has been recently reported for $NaGdF_4$-based nanoparticles that r_1 increased with decreasing particle size probably due to a major contribution of the surface Gd ions to relaxation of water protons when compared to that of those located in the bulk.[2g] As a consequence of the low r_1 value the r_2/r_1 ratio for our nanoparticles becomes high, precluding their use as positive contrast agent.[2g,10a] However, the MRI phantom analysis (Figure.9) clearly manifested T_2 susceptibility effects at higher

dx.doi.org/10.1021/ic3016996 | Inorg. Chem. 2013, 52, 647−654

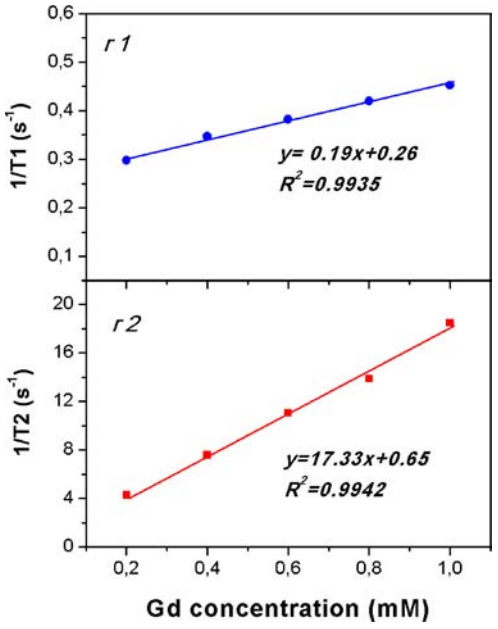

Figure 8. Proton relaxivities (r_1 and r_2) measured for the $Eu_{0.02}Gd_{0.98}PO_4$ nanophosphor at 0.47 T.

magnetic field (9.4 T), indicating that our Eu:$GdPO_4$ nanocubes are suitable as negative (T_2-weighted) MRI contrast agent.

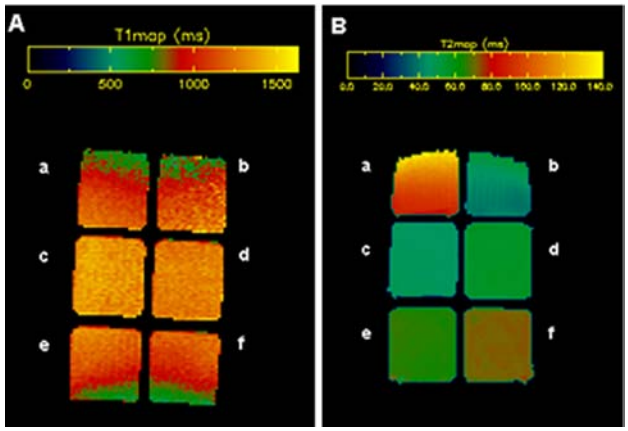

Figure 9. T_1 (A) and T_2 (B) parametric MRI phamtom images (9.4 T) of the $Eu_{0.02}Gd_{0.98}PO_4$ nanophosphor showing longitudinal and transversal relaxation times, respectively, of nanoparticle solutions: (a) control (water) and (b–f) serial dilutions.

Biocompatibility studies of the Eu:$GdPO_4$ nanocubes were undertaken by evaluating the cell viability of Vero cells by the MTT assay after 24 h treatment with the nanocubes. Negligible toxicity effects were observed for concentrations up to 0.5 mg cm^{-1} (Figure 10).

CONCLUSIONS

The microwave-assisted heating at 120 °C for at least 7 min of 0.02 mol dm^{-3} gadolinium acetylacetonate and 0.15 mol dm^{-3} phosphoric acid solutions in butylene glycol yields uniform gadolinium phosphate nanocubes (edge = 75 nm). These nanocubes are highly crystalline and crystallize into a tetragonal structure, which has not been ever reported for pure gadolinium phosphate. This crystal structure has been

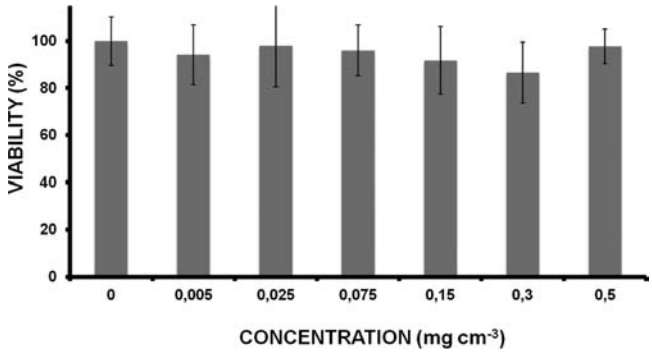

Figure 10. Cytotoxicity profiles of nanoparticles with VERO cells as determined by MTT assay. Percentage of viability of cells was expressed relative to control cells (n = 5). Results are represented as mean ± standard deviations.

determined here by means of powder X-ray diffraction, finding that this compound is isostructural with the pure lanthanide orthophosphates having zircon structure. This synthesis procedure is also successful for preparation of multifunctional europium(III)-doped gadolinium phosphate nanocubes similar to those of the undoped sample, which exhibit the strongest red luminescence for an Eu content of 2% (Eu/Eu+Gd mol ratio). These nanoparticles are nontoxic for cells and present high transverse relaxivity (r_2) values. These properties make the here synthesized Eu:$GdPO_4$ nanocubes suitable as biolabels for in vitro optical imaging and negative contrast agent for magnetic resonance imaging.

ASSOCIATED CONTENT

Supporting Information

TEM micrograph (a) and XRD pattern (b) of the $GdPO_4$ sample prepared by heating at 120 °C for 1 h, DEG solutions containing 0.02 mol dm^{-3} $Gd(acac)_3$ and 0.15 mol dm^{-3} H_3PO_4 using a conventional oven, TEM micrograph (a) and XRD pattern (b) of the $GdPO_4$ sample prepared by heating at 120 °C for 1 h, 0.02 mol dm^{-3} $Gd(acac)_3$ and 0.15 mol dm^{-3} H_3PO_4 solutions in EG, using a microwave oven, TEM micrographs of the $GdPO_4$ samples prepared by heating at 120 °C for 1 h in a microwave oven, EG solutions containing 0.15 mol dm^{-3} H_3PO_4 and different concentrations of $Gd(acac)_3$, TEM image of the nanoparticles prepared by heating at 120 °C for 1 h in a microwave oven, DEG solutions containing H_3PO_4 (0.15 mol dm^{-3}), $Eu(acac)_3$, and $Gd(acac)_3$ (Gd + Eu = 0.02 mol dm^{-3}, Eu/Eu+Gd molar ratio = 10%), TGA curve obtained for the $Eu_{0.05}Gd_{0.95}PO_4$ sample. This material is available free of charge via the Internet at http://pubs.acs.org.

AUTHOR INFORMATION

Corresponding Author

*E-mail: mjurado@icmse.csic.es.

Notes

The authors declare no competing financial interest.

ACKNOWLEDGMENTS

This work was supported by Junta de Andalucía (Grant FQM6090), the Spanish CICYT (Grant MAT2011-23593), ERC-Starting Grant NANOPUZZLE (ERC-StG-2009-239931), and Marie Curie Action IOF-MRI_Nanobiosensors. J.M.F. wants to thank ARAID for financial support. S.R.L. wants to thank the Spanish Ministerio de Ciencia y Tecnología for an

FPI fellowship. Authors thank M. L. Garcia Martin for fruitful discussion and I. Echaniz for technical support.

REFERENCES

(1) (a) Yoon, T. J.; Kim, J. S.; Kim, B. G.; Yu, K. N.; Cho, M.-H.; Lee, J.-K. *Angew. Chem., Int. Ed.* **2005**, *44*, 1068. (b) Kim, J.; Lee, J. E.; Lee, J.; Yu, J. H.; Kim, B. C.; An, K.; Hwang, Y.; Shin, C.-H.; Park, J.-G.; Kim, J.; Hyeon, T. *J. Am. Chem. Soc.* **2006**, *128*, 688. (c) Liong, M.; Lu, J.; Kovochich, M.; Xia, T.; Ruehm, S. G.; Nel, A. E.; Tamanoi, F.; Zink, J. *ACS Nano* **2008**, *2*, 889. (d) Zhang, F.; Braun, G. B.; Pallaoro, A.; Zhang, Y.; Shi, Y.; Cui, D.; Moskovits, M.; Zhao, D.; Stucky, G. D. *Nano Lett.* **2012**, *12*, 61. (e) Tian, G.; Gu, Z.; Liu, X.; Zhou, L.; Yin, W.; Yan, L.; Jin, S.; Ren, W.; Xing, G.; Li, S.; Zhao, Y. *J. Phys. Chem. C* **2011**, *115*, 23790. (f) Luwang, M. N.; Chandra, S.; Bahadur, D.; Srivastava, S. K. *J. Mater. Chem.* **2012**, *22*, 3395.

(2) (a) Mulder, W. JM.; Griffioen, A. W.; Strijkers, G. J.; Cormode, D. P.; Nicolay, K.; Fayad, Z. A. *Nanomedicine* **2007**, *2*, 307. (b) Kumar, R.; Nyk, M.; Ohulchanskyy, T. Y.; Flask, C. A.; Prasad, P. N. *Adv. Funct. Mater.* **2009**, *19*, 853. (c) Das, G. K; Heng, B. C.; Ng, S.-C.; White, T.; Loo, J. S. C.; D'Silva, L.; Padmanabhan, P.; Bhakoo, K. K.; Selvan, S. T.; Tan, T. T. Y. *Langmuir* **2010**, *26* (11), 8959. (d) Ryu, J.; Park, H.-Y.; Kim, K.; Kim, H.; Yoo, J. H; Kang, M.; Im, K.; Grailhe, R.; Song, R. *J. Phys. Chem.C* **2010**, *114*, 21077. (e) Park, Y. I.; Kim, J. H.; Lee, K. T.; Jeon, K.-S.; Na, H. B.; Yu, J. H.; Kim, H. M.; Lee, N.; Choi, S. H.; Baik, S.-I; Kim, H.; Park, S. P.; Park, B.-J.; Kim, Y. W.; Lee, S. H.; Yoon, S.-Y.; Song, I. C; Moon, W. K.; Suh, Y. D.; Hyeon, T. *Adv. Mater.* **2009**, *21*, 4467. (f) Yu, X.; Shan, Y.; Li, G.; Chen, K. *J. Mater. Chem.* **2011**, *21*, 8104. (g) Johnson, N. J. J.; Oakden, W.; Stanisz, G. J.; Prosser, R. S.; van Veggel, F. C. J. M. *Chem. Mater.* **2011**, *23*, 3714. (h) He, M.; Huang, P.; Zhang, C.; Hu, H.; Bao, C.; Gao, G.; He, R.; Cui, D. *Adv. Funct. Mater.* **2011**, *21*, 4470. (i) Zhou, L.; Gu, Z.; Liu, X.; Yin, W.; Tian, G.; Yan, L.; Jin, S.; Ren, W.; Xing, G.; Li, W.; Chang, X.; Hu, Z.; Zhao, Y. *J. Mater. Chem.* **2012**, *22*, 966.

(3) Liu, Z.; Yi, G.; Zhang, H.; Ding, J.; Zhang, Y.; Xue, J. *Chem. Commun.*. **2008**, 694.

(4) Zhang, Y.; Das, G. K.; Xu, R.; Tan, T. T. *J. Mater. Chem.* **2009**, *19*, 3696.

(5) Wang, F.; Chen, X.; Zhao, Z.; Tang, S.; Huang, X.; Lin, C.; Cai, C.; Zheng, N. *J. Mater. Chem.* **2011**, *21*, 11244.

(6) Ma, Z. Y.; Dosev, D.; Nichkova, M.; Gee, S. J.; Hammock, B. D.; Kennedy, I. M. *J. Mater. Chem.* **2009**, *19*, 4695.

(7) Bridot, J. L; Faure, A.-C; Laurent, S.; Rivière, C.; Billotey, C.; Hiba, B.; Janier, M.; Josserand, V.; Coll, J.-J.; Elst, L. V.; Muller, R.; Roux, S.; Perriat, P.; Tillement, O. *J. Am. Chem. Soc.* **2007**, *129*, 5076.

(8) Evanics, F.; Diamente, P. R.; van Veggel, F. C. J. M.; Stanisz, G. J.; Prosser, R. S. *Chem. Mater.* **2006**, *18*, 2499.

(9) Taylor, K. M. L.; Kim, J. S.; Rieter, W. J.; An, H.; Lin, W.; Lin, W. *J. Am. Chem. Soc.* **2008**, *130*, 2154.

(10) (a) Hifumi, H.; Yamaoka, S.; Tanimoto, A.; Citterio, D.; Suzuki, K. *J. Am. Chem. Soc.* **2006**, *128*, 15090. (b) Dumont, M. F.; Baligand, C.; Li, Y.; Knowles, E.; Meisel, M. W.; Walter, G. A.; Talham, D. R. *Bioconjugate Chem.* **2012**, *23*, 951. (c) Ren, W.; Tian, G.; Zhou, L.; Yin, W.; Yan, L.; Jin, S.; Zu, Y.; Li, S.; Gu, Z.; Zhao, Y. *Nanoscale* **2012**, *4*, 3754.

(11) (a) Zhang, Y. W.; Yan, Z. G.; You, L. P.; Si, R.; Yan, C. H. *Eur. J. Inorg. Chem.* **2003**, 4099. (b) Yan, R.; Sun, X.; Wang, X.; Peng, Q.; Li, Y. *Chem.—Eur. J.* **2005**, *11*, 2183. (c) Di, W.; Wang, X.; Zhao, H. *J. Nanosci. Nanotechnol.* **2007**, *7*, 3624. (d) Huang, C. C.; Lo, Y. W.; Kuo, W. S.; Hwu, J. R.; Su, W. C.; Shieh, D. B.; Yeh, C. S. *Langmuir* **2008**, *24*, 8309. (e) Yan, B.; Gu, J.; Xiao, X. *J. Nanopart. Res.* **2010**, *12*, 2145.

(12) (a) Kim, T. W.; Chung, P. W.; Slowing, I. I.; Tsunoda, M.; Yeung, E. S.; Lin, V. S. Y. *Nano Lett.* **2008**, *10*, 3724. (b) Kim, D. K.; Dobson, J. *J. Mater. Chem.* **2009**, *19*, 6294.

(13) Huo, Z.; Chen, C.; Chu, D.; Li, H.; Li, Y. *Chem.—Eur. J.* **2007**, *13*, 7708.

(14) Yaiphaba, N.; Ningthoujam, R. S.; Singh, N. R.; Vatsa, R. K. *Eur. J. Inorg. Chem.* **2010**, 2682.

(15) Ni, Y.; Hughes, J. M.; Mariano, A. N. *Am. Mineral.* **1995**, *80*, 21.

(16) Milligan, W. O.; Mullica, D. F.; Beall, G. W.; Boatner, L. A. *Inorg. Chim. Acta* **1983**, *70*, 133.

(17) Mosmann, T. J. *J. Immunol. Methods* **1993**, *95*, 55.

(18) Matijević, E. *Chem. Mater.* **1993**, *5*, 412.

(19) Rodriguez-Liviano, S.; Aparicio, F. J.; Rojas, T. C.; Hungría, A. B.; Chinchilla, L. E.; Ocaña, M. *Cryst. Growth Des.* **2012**, *12*, 635.

(20) Zhu, X. X.; Zhang, Q. H.; Li, Y. G.; Wang, H. Z. *J. Mater. Chem.* **2010**, *20*, 1766.

(21) (a) Feldmann, C. *Adv. Funct. Mater.* **2003**, *13*, 101. (b) Poul, L.; Ammar, S.; Jouini, N.; Fievet, F. *J. Sol-Gel Sci. Technol.* **2003**, *26*, 261.

(22) Ito, H.; Fujishiro, Y.; Sato, T.; Okuwaki, A. *Br. Ceram. Trans.* **1995**, *94*, 146.

(23) (a) Milligan, W. O.; Mullica, D. F.; Beall, G. W.; Boatner, L. A. *Inorg. Chim. Acta* **1982**, *60*, 39. (b) Milligan, W. O.; Mullica, D. F. *Acta Crystallogr., Sect. C* **1983**, *39*, 23.

(24) Mullica, D. F.; Grossie, D. A.; Boatner, L. A. *Inorg. Chim. Acta* **1986**, *118*, 173.

(25) Mullica, D. F.; Sappenfield, E. L.; Boatner, L. A. *Inorg. Chim. Acta* **1990**, *174*, 155.

(26) Mullica, D. F.; Sappenfield, E. L.; Boatner, L. A. *J. Solid State Chem.* **1992**, *99*, 313.

(27) Vegard, L. *Philos. Mag.* **1927**, *4*, 511

(28) Shannon, R. D. *Acta Crystallogr.* **1976**, *A32*, 751.

(29) Zhang, L.; Yin, M.; You, H.; Yang, M.; Song, Y.; Huang, Y. *Inorg. Chem.* **2011**, *50*, 10608.

(30) Yaiphaba, N.; Ningthoujam, R. S.; Singh, N. S.; Vatsa, R. K.; Singh, N. R.; Dhara, S.; Misra, N. L.; Tewari, R. *J. Appl. Phys.* **2010**, *107*, 34301.